

What measurements of neutrino neutral current events can reveal

Raj Gandhi,^a Boris Kayser,^b Suprabh Prakash,^c Samiran Roy^a

^a*Harish-Chandra Research Institute, HBNI, Chhatnag Road, Jhansi, Allahabad 211019, India*

^b*Theoretical Physics Department, Fermilab, P.O. Box 500, Batavia, IL 60510 USA*

^c*Instituto de Física Gleb Wataghin - UNICAMP, 13083-859, Campinas, São Paulo, Brazil*

E-mail: raj@hri.res.in, boris@fnal.gov, samiranroy@hri.res.in,
sprakash@ifi.unicamp.br

ABSTRACT: We show that neutral current (NC) measurements at neutrino detectors can play a valuable role in the search for new physics. Such measurements have certain intrinsic features and advantages that can fruitfully be combined with the usual well-studied charged lepton detection channels in order to probe the presence of new interactions or new light states. In addition to the fact that NC events are immune to uncertainties in standard model neutrino mixing and mass parameters, they can have small matter effects and superior rates since all three flavours participate. We also show, as a general feature, that NC measurements provide access to different combinations of CP phases and mixing parameters compared to CC measurements at both long and short baseline experiments. Using the Deep Underground Neutrino Experiment (DUNE) as an illustrative setting, we demonstrate the capability of NC measurements to break degeneracies arising in CC measurements, allowing us, in principle, to distinguish between new physics that violates three flavour unitarity and that which does not. Finally, we show that NC measurements can enable us to restrict new physics parameters that are not easily constrained by CC measurements.

Contents

1	Introduction	1
2	Neutral current events in new physics scenarios with CP violation: a general property	4
3	Neutral current and new physics at long baselines	5
3.1	An approximate analytical expression for $P_{\mu s}$	7
3.2	Effect of the CP violating phases on P_{NC}	9
4	Neutral current measurements as a tool to break BSM physics degeneracies	12
5	Constraints on the 3+1 paradigm: Sensitivity forecasts with DUNE	14
6	Summary and concluding remarks	18

1 Introduction

The major goals of present-day and near-future neutrino oscillation experiments are: a) the determination of the neutrino mass hierarchy (MH) and b) the discovery and possible measurement of the magnitude of CP violation (CPV) in the lepton sector. In addition, ancillary goals include making increasingly precise determinations of neutrino mass-squared differences, $\delta m_{ij}^2 = m_i^2 - m_j^2$ ($i, j = 1, 2, 3$ & $i \neq j$) and mixing angles θ_{ij} . Recent status reviews may be found in [1–3].

The capability for increased precision in neutrino experiments has recently led to the formulation of another important line of inquiry: the search for new physics at neutrino detectors, and its identification and disentanglement from physics related to the standard model with three generations of massive neutrinos. Examples of recent work in this direction may be found in [4–41]. It is the purpose of this work to bring out facets of neutral current (NC) measurements at neutrino detectors that can aid in furthering efforts in this direction either on their own or when employed in synergy with other measurements.

Most investigations for new physics at long or short baseline neutrino experiments have focussed on measurements made using the charged current (CC) channels, with either $\nu_\mu \rightarrow \nu_e$ or $\nu_\mu \rightarrow \nu_\mu$ as the underlying probabilities, and a final state electron or muon respectively. Our purpose in this paper is to study the potential of neutrino NC events at such experiments to provide a tool to investigate features of new physics scenarios. This category of neutrino interactions in a typical detector fed by a neutrino beam generated in an accelerator facility can comprise neutrino-nucleon and neutrino-electron elastic scattering, neutrino deep-inelastic scattering, neutrino-nucleon resonant scattering with a pion in

the final state, and finally, neutrino coherent pion scattering¹. Similar processes exist, of course, for anti-neutrinos. The relative contributions from these various channels depend on the detector medium, the cross section and the energy of the beam, among other things.

As we shall show in the remainder of the paper, the measurement and study of NC events can in some cases provide a qualitatively different, complementary and statistically superior handle on neutrino properties in new physics scenarios compared to CC measurements. Even when making measurements without the presumption of any new physics, these differences and complementarity can be useful. To see this, we consider Fig. 1, which assumes the 3+0 scenario. This figure shows, in the left panel, the full 3σ allowed possible band of CC electron events at the DUNE far detector given our present knowledge of three generation neutrino parameters². The hierarchy is treated as being unknown, and the mixing angles and the CP phase are varied in their presently allowed ranges. Clearly, any measurement by DUNE in this large band is currently acceptable as being consistent with the standard model with massive neutrinos, given the present three flavour parameter ranges. The right panel shows the NC events for the same parameter variations³. Besides the superior statistics, we note the lack of any dependence on the parameter uncertainties. The reason for this is, of course, the fact that the NC rate is insensitive to any flavour oscillations given the universality of weak interactions. A significant deviation from the rate shown, if detected, would clearly indicate the presence of certain kinds of new physics (as we discuss later in the paper), as opposed to the CC rate which is encumbered by significant uncertainty as well as the possibility of degeneracy between new and standard physics.

In subsequent sections, we first emphasise and bring out a general property of CC versus NC event measurements which can be useful in new physics settings with CP violation at both long and short baselines. We show, in a general way, that NC and CC measurements complement each other in providing information on CP phases and mixing angles. Then, using the 3+1 scenario⁴ at DUNE as an exemplar, we derive an approximate analytic expression for the probability governing NC event rates in vacuum, and discuss its features. We find that the effects of matter on NC event rates are small, allowing us to use the vacuum expression to good effect.

We find that NC measurements can be revealing in several ways; for instance, we

¹NC resonant pion scattering in DUNE can comprise the processes $\nu_\mu p \rightarrow \nu_\mu p \pi^0 (n\pi^+)$ and $\nu_\mu n \rightarrow \nu_\mu n \pi^0 (p\pi^-)$. NC coherent pion scattering from a target nucleus A is the process $\nu_\mu A \rightarrow \nu_\mu A \pi^0$.

² Throughout this work, we have used the GLOBES software package [42, 43] along with the `snu.c` routine [44, 45] to generate probability, events, and to do $\Delta\chi^2$ -level analyses.

³As explained in Sec. 3, we use migration matrices provided to us by Michel Sorel to relate reconstructed visible energy in NC events in DUNE to true energy. We note that in the reconstructed energy spectrum in Fig. 1, and also later in the paper in the right panel of Fig. 7, there is a small but somewhat surprising dip between 200 and 300 MeV. We thank Dr. Sorel for checking that this dip is indeed produced by the migration matrices. Since these matrices incorporate many physics details, it is difficult to pin down the origin of the dip more precisely. However, our conclusions are not affected by this dip.

⁴This is dictated less by a belief in the veracity of 3+1 as nature's choice of physics beyond the standard model and more by the fact that it offers a simple template enabling us to bring out features and draw conclusions which may have applicability to other more complex new physics scenarios. Indeed, recent constraints restrict the allowed 3+1 parameter space significantly, as we discuss in Sec. 3.

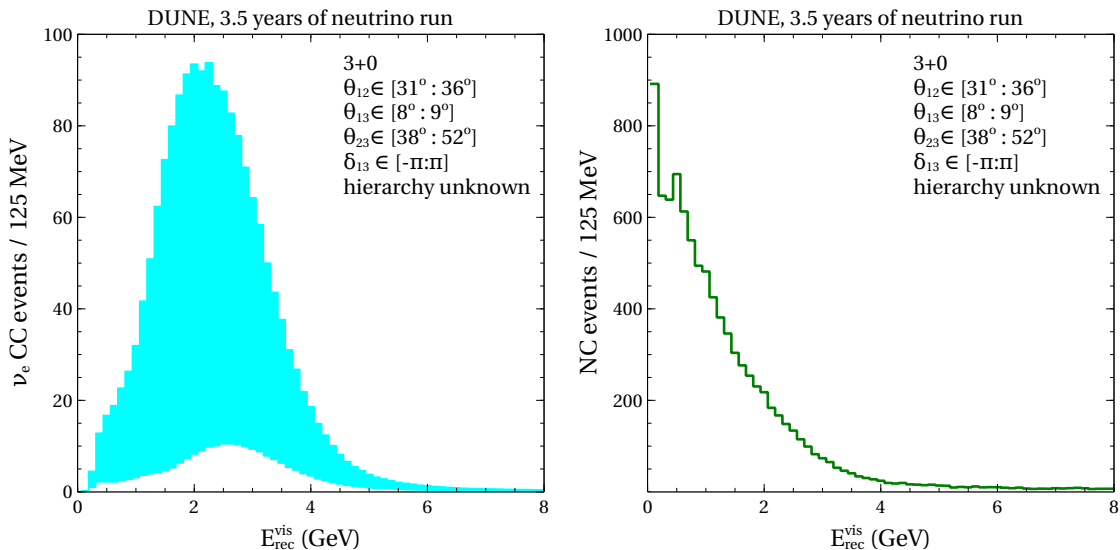


Figure 1: The left and right panel correspond to ν_e CC and NC events respectively. Here, all parameters are varied in their currently allowed range. $E_{\text{rec}}^{\text{vis}}$ represents the reconstructed visible energy of the events in the detector. In the case of CC events, it closely matches the true energy of the incoming neutrino. For the NC events, $E_{\text{rec}}^{\text{vis}}$ can be very different from the true incoming neutrino energy, as we discuss later.

show that some CP-violating phase combinations lead to significant effects on the neutrino and anti-neutrino NC probabilities, although not to a significant CP-violating difference between them. Nevertheless, we find that under some circumstances there is good sensitivity to these phases. We provide bi-probability plots of neutrino versus anti-neutrino NC probabilities for fixed mixing angles to show that the CP phases can have substantial effects. We discuss how NC events break the degeneracy present in CC events, allowing us to discriminate new physics associated with new sterile states from that associated with non-standard interactions in neutrino propagation. We identify the general category of new physics scenarios which lend themselves to such degeneracy breaking via NC events. Using the 3+1 scenario as an example, we show the efficacy of NC events in constraining parameters and discuss how they can help improve existing bounds.

Finally, it bears noting that since all three flavours contribute, NC event measurements are typically statistically rich. For instance, in the Deep Underground Neutrino Experiment (DUNE), a 7-ton fine-grained tracking near detector at ~ 500 m is planned, and it is expected to detect in excess of 400000 NC current events in a year [46]. Similar considerations would hold for the planned Short-Baseline Neutrino (SBN) program at Fermilab [47, 48]. Even at long baselines, NC events are typically higher in number compared to any one measured CC channel, which buttresses the significance of any conclusions based on their measurement.

2 Neutral current events in new physics scenarios with CP violation: a general property

This section identifies a salient property of the NC probability, P_{NC} , defined as $\sum_{\beta} P(\alpha \rightarrow \beta)$, $\alpha, \beta = e, \mu, \tau$ for a given neutrino source beam of flavour α and an assumed physics scenario, which will actively contribute to the measured NC rate. In the standard $3 + 0$ scenario, for instance, given a source beam of primarily muon neutrinos and the universality of weak interactions, $P_{NC} = P_{\mu e} + P_{\mu \tau} + P_{\mu \mu} = 1$. For the same source beam, but an assumed $3+1$ scenario, $P_{NC} = 1 - P_{\mu s} = P_{\mu e} + P_{\mu \tau} + P_{\mu \mu} \neq 1$, where s denotes the sterile flavour. This section is focussed on bringing out a feature of NC events that is generic to new physics scenarios with CP violation, assuming a $3+2$ scenario at a short baseline as an example.

In general, useful conclusions regarding the properties of P_{NC} can be drawn by examining analytic expressions and comparing them to expressions for their corresponding CC counterparts, *e.g.* $P_{\mu e}$. We begin by writing down a general expression for the flavour oscillation probability in vacuum,

$$P(\alpha \rightarrow \beta) = \delta_{\alpha\beta} - 4Re \sum_{k>j} (U_{\alpha k}^* U_{\beta k} U_{\alpha j} U_{\beta j}^*) \sin^2 \Delta_{kj} + 2Im \sum_{k>j} (U_{\alpha k}^* U_{\beta k} U_{\alpha j} U_{\beta j}^*) \sin 2\Delta_{kj}. \quad (2.1)$$

Here k, j run over the mass eigenstates, whereas α, β denote flavours. Additionally, $\Delta_{kj} = 1.27 \times \delta m_{kj}^2 [\text{eV}^2] \times L [\text{km}] / E [\text{GeV}]$ where L is the baseline length and E is the neutrino energy. Eq. 2.1 is valid for any number of flavours (including sterile ones, if present).

Consider an experiment sourced by an accelerator generated ν_{μ} beam, and a $3+2$ scenario, with two additional sterile flavour states ν_{s_1} and ν_{s_2} , and mass eigenstates ν_4 and ν_5 . From Eq 2.1, we see that the CP violating part of $P_{\mu s_1}$ resides in

$$P_{\mu s_1}^{CP} \propto Im \sum_{k>j} (U_{\mu k}^* U_{s_1 k} U_{\mu j} U_{s_1 j}^*) \sin 2\Delta_{kj} \simeq Im [U_{\mu 5}^* U_{s_1 5} (U_{\mu 4} U_{s_1 4}^* \sin 2\Delta_{54} + U_{\mu 3} U_{s_1 3}^* \sin 2\Delta_{53} + U_{\mu 2} U_{s_1 2}^* \sin 2\Delta_{52} + U_{\mu 1} U_{s_1 1}^* \sin 2\Delta_{51}) + U_{\mu 4}^* U_{s_1 4} (U_{\mu 3} U_{s_1 3}^* \sin 2\Delta_{43} + U_{\mu 2} U_{s_1 2}^* \sin 2\Delta_{42} + U_{\mu 1} U_{s_1 1}^* \sin 2\Delta_{41}) + U_{\mu 3}^* U_{s_1 3} (U_{\mu 2} U_{s_1 2}^* \sin 2\Delta_{32} + U_{\mu 1} U_{s_1 1}^* \sin 2\Delta_{31}) + U_{\mu 2}^* U_{s_1 2} (U_{\mu 1} U_{s_1 1}^* \sin 2\Delta_{21})] \quad (2.2)$$

A similar expression can be written down for $P_{\mu s_2}^{CP}$ with s_1 replaced by s_2 everywhere, leading to

$$P_{NC} = 1 - P_{\mu s_1} - P_{\mu s_2}.$$

For a short baseline (SBL) experiment, the terms proportional to $\sin 2\Delta_{ij}$, with $i, j =$

1, 2, 3 can be dropped in comparison to the others, and $P_{\mu s_{1,2}}$ simplify; for instance,

$$\begin{aligned}
P_{\mu s_1}^{CP} &\simeq \text{Im} \left[U_{\mu 5}^* U_{s_1 5} \left(U_{\mu 4} U_{s_1 4}^* \sin 2\Delta_{54} \right. \right. \\
&\quad + U_{\mu 3} U_{s_1 3}^* \sin 2\Delta_{53} + U_{\mu 2} U_{s_1 2}^* \sin 2\Delta_{52} + U_{\mu 1} U_{s_1 1}^* \sin 2\Delta_{51} \left. \right) \\
&\quad \left. + U_{\mu 4}^* U_{s_1 4} \left(U_{\mu 3} U_{s_1 3}^* \sin 2\Delta_{43} + U_{\mu 2} U_{s_1 2}^* \sin 2\Delta_{42} + U_{\mu 1} U_{s_1 1}^* \sin 2\Delta_{41} \right) \right].
\end{aligned} \tag{2.3}$$

For this scenario, the CP violating part of the CC probability, under the same approximation as Eq. 2.3, is proportional to

$$\begin{aligned}
P_{\mu e}^{CP} &\propto \text{Im} \sum_{k>j} (U_{\mu k}^* U_{ek} U_{\mu j} U_{ej}^*) \sin 2\Delta_{kj} \\
&\simeq \text{Im} \left[U_{\mu 5}^* U_{e5} \left(U_{\mu 4} U_{e4}^* \sin 2\Delta_{54} + U_{\mu 3} U_{e3}^* \sin 2\Delta_{53} + U_{\mu 2} U_{e2}^* \sin 2\Delta_{52} + U_{\mu 1} U_{e1}^* \sin 2\Delta_{51} \right) \right. \\
&\quad \left. + U_{\mu 4}^* U_{e4} \left(U_{\mu 3} U_{e3}^* \sin 2\Delta_{43} + U_{\mu 2} U_{e2}^* \sin 2\Delta_{42} + U_{\mu 1} U_{e1}^* \sin 2\Delta_{41} \right) \right].
\end{aligned} \tag{2.4}$$

In a scenario geared towards explaining the short baseline anomalies [49–53], further simplifications are possible, *e.g.* $\delta m_{lm}^2 \gg \delta m_{mn}^2$, $l = 4$ or $l = 5$, $m, n = 1, 2, 3$ ⁵. After a little algebra, one then finds that the CP violating difference between NC events measured using an initially muon-flavoured neutrino beam, and those measured using its anti-neutrino counterpart, will be proportional to the quantity D_{NC} , given by

$$D_{NC} \propto \text{Im} \left[U_{\mu 5}^* U_{\mu 4} \left(U_{s_1 5} U_{s_1 4}^* + U_{s_2 5} U_{s_2 4}^* \right) \right] \sin \Delta_{54} \sin \Delta_{43} \sin \Delta_{53}. \tag{2.5}$$

On the other hand, the analogous difference for CC events from $\nu_\mu \rightarrow \nu_e$ transitions is proportional to

$$D_{CC} \propto \text{Im} \left[U_{\mu 5}^* U_{\mu 4} U_{e5} U_{e4}^* \right] \sin \Delta_{54} \sin \Delta_{43} \sin \Delta_{53}. \tag{2.6}$$

Comparing Eq. 2.3 with Eq. 2.4 and Eq. 2.5 with Eq. 2.6, we see that in both cases they tap into different CP phases and sectors of the mixing matrix. Consequently, the NC measurements will provide a qualitatively and quantitatively different window into the CP violating and mixing sectors of a new physics scenario compared to the CC measurements. Should a new physics scenario with CP violation be nature’s choice, then combining NC measurements with CC measurements would provide a valuable way to probe it.

3 Neutral current and new physics at long baselines

For the remainder of this paper, we focus largely, but not exclusively, on the 3+1 scenario in order to study the potential of NC events as a probe and diagnostic tool for new physics.

Additionally, we perform our calculations for the DUNE far detector. DUNE [46] is a proposed future super-beam experiment with the main aim of establishing or refuting the existence of CPV in the leptonic sector. In addition to this primary goal, this facility will

⁵We stress that the general conclusion we draw in this section remains unchanged with or without such simplifications.

also be able to resolve the other important issues like the mass hierarchy and the octant of θ_{23} . The $\nu_\mu(\bar{\nu}_\mu)$ super-beam will originate at the Fermilab. The optimised beam simulation assumes a 1.07 MW - 80 GeV proton beam which will deliver 1.47×10^{21} protons-on-target (POT) per year. A 40 kt Liquid Argon (LAr) far-detector will be placed in the Homestake mine in South Dakota, 1300 km away. The experiment plans to have a total of 7 years of running, divided equally between neutrinos and anti-neutrinos, corresponding to a total exposure of 4.12×10^{23} kt-POT-yr. The complete experimental description of the DUNE experiment such as the CC signal and background definitions as well as assumptions on the detector efficiencies concerning the CC events are from [54]. The details regarding the anticipated NC events at DUNE were taken from [55]. The NC event detection efficiency has been assumed to be 90%. In order to correctly reproduce the NC events spectra, we have made use of the *migration matrices*. In a NC event, the outgoing (anti-)neutrino carries away some fraction of the incoming energy. This energy is missed and hence, the reconstructed visible energy is less than the total incoming energy. As such, the events due to energetic (anti-)neutrinos are reconstructed inaccurately at lower visible energies in a majority of such cases⁶. Therefore, using a gaussian energy resolution function in such a situation is not appropriate. We have used the migration matrices from [56], provided to us by [57]. Note that these migration matrices correspond to a binning of 50 MeV and therefore, in this work too, we have considered the energy bins of 50 MeV for NC events⁷. For the analysis of CC events, we have used energy bins of 125 MeV as in [54]. The background to NC events consists of CC events that get mis-identified as NC events. These include electron events (due to CC signal $\nu_\mu \rightarrow \nu_e$ or intrinsic beam $\nu_e \rightarrow \nu_e$), muon events ($\nu_\mu \rightarrow \nu_\mu$), tau events ($\nu_\mu \rightarrow \nu_\tau$) and their respective CP-reversed channels due to anti-neutrino/neutrino contaminations in the beam. It should be noted that the backgrounds too, will oscillate into the sterile flavour depending on the values of U_{e4} , $U_{\mu4}$ and $U_{\tau4}$. In such a scenario, the simplifying assumptions of putting one or more of these matrix elements to 0, *may not* give the correct estimate of the NC signal events. For the NC analysis, the signal and background normalisation errors have been taken to be 5% and 10% respectively.

Finally, we note that in the 3+1 scenario, flavor oscillations may lead to some depletion of the active neutrino flux and of its muon neutrino component at the location of the DUNE near detector (~ 500 m). This could, in principle, distort the flux measurement made at this location, which forms the basis of conclusions drawn regarding oscillations measured at the far detector. We have assumed an overall error of 5% in flux measurements, and have checked that given the currently allowed parameter ranges for the 3+1 scenario, the change in flux due to a sterile species is always below this limit. On the other hand, as we show in this work, depletion in the NC rate significantly above this uncertainty is expected at the far detector, hence enabling DUNE to detect the possible presence of a sterile state via neutral current measurements.

⁶The profile of NC events spectrum, for example, can be seen in the right panel of Fig. 1.

⁷For the sake of clarity, we show NC events in Figs. 1 and 7 in energy bins of 125 MeV. However, for binned- $\Delta\chi^2$ calculations, we have considered 50 MeV energy bins.

3.1 An approximate analytical expression for $P_{\mu s}$

As mentioned above, the NC rate in a 3 + 1 scenario will be proportional to $1 - P_{\mu s}$. We give below a useful approximate expression, starting from Eq. 2.1, since the full expression which follows from it is extremely long and complicated. In obtaining this approximate form, we have adopted the following parameterisation for the PMNS matrix:

$$U_{\text{PMNS}}^{3+1} = O(\theta_{34}, \delta_{34})O(\theta_{24}, \delta_{24})O(\theta_{14})O(\theta_{23})O(\theta_{13}, \delta_{13})O(\theta_{12}) \quad (3.1)$$

Here, in general, $O(\theta_{ij}, \delta_{ij})$ is a rotation matrix in the ij sector with associated phase δ_{ij} . For example,

$$O(\theta_{24}, \delta_{24}) = \begin{pmatrix} 1 & 0 & 0 & 0 \\ 0 & \cos \theta_{24} & 0 & e^{-i\delta_{24}} \sin \theta_{24} \\ 0 & 0 & 1 & 0 \\ 0 & e^{i\delta_{24}} \sin \theta_{24} & 0 & \cos \theta_{24} \end{pmatrix}; \quad O(\theta_{14}) = \begin{pmatrix} \cos \theta_{14} & 0 & 0 & \sin \theta_{14} \\ 0 & 1 & 0 & 0 \\ 0 & 0 & 1 & 0 \\ -\sin \theta_{14} & 0 & 0 & \cos \theta_{14} \end{pmatrix} \text{ etc.}$$

Measurements from MINOS, MINOS+, Daya Bay and the IceCube experiments provide significant constraints on the 3+1 paradigm. See, for instance, [58–60]. The Super-Kamiokande data, MINOS NC data, NO ν A NC data and the IceCube-DeepCore data provide constraints on the 3-4 mixing [61–64]. Our work in this paper utilises only the currently allowed parameter space for this scenario as determined by these references⁸. Since these current constraints restrict $\theta_{13}, \theta_{14}, \theta_{24} \leq 13^\circ$, we take $\sin^3 \theta_{ij} = 0$, where θ_{ij} is any of these angles. We also set $\theta_{23} = 45^\circ$ for simplicity, and assume $\sin^2 \frac{\Delta m_{31}^2 L}{4E} = \sin^2 \frac{\Delta m_{32}^2 L}{4E}$, while neglecting the contribution from the solar mass-squared difference, since $\Delta m_{21}^2 \ll \Delta m_{31}^2$. Additionally, we work under the assumption that the mass-squared differences δm_{lm}^2 , $l = 4$, $m = 1, 2, 3$ are all approximately equal, implying that the fourth mass eigenstate is much heavier than the other three. With these simplifications, we obtain, for the vacuum transition probability for ν_μ to ν_s ,

$$\begin{aligned} P_{\mu s}^{\text{vac}} &\simeq \cos^4 \theta_{14} \cos^2 \theta_{34} \sin^2 2\theta_{24} \sin^2 \frac{\Delta m_{41}^2 L}{4E} \\ &+ \left[\cos^4 \theta_{13} \cos^2 \theta_{24} \sin^2 \theta_{34} - \cos^2 \theta_{13} \cos^2 \theta_{24} \cos^2 \theta_{34} \sin^2 \theta_{24} \right. \\ &+ \left. \frac{1}{\sqrt{2}} \sin 2\theta_{13} \sin 2\theta_{34} \sin \theta_{14} \cos^3 \theta_{24} \cos(\delta_{13} + \delta_{34}) \right] \sin^2 \frac{\Delta m_{31}^2 L}{4E} \\ &+ \frac{1}{2} \cos^2 \theta_{13} \cos^2 \theta_{24} \sin 2\theta_{34} \sin \theta_{24} \sin(\delta_{34} - \delta_{24}) \sin \frac{\Delta m_{31}^2 L}{2E}. \end{aligned} \quad (3.2)$$

Prior to testing the accuracy of this formula and determining its applicability, we note the following characteristics:

⁸It should be noted that there are global analyses of the existing oscillation data that provide constraints on the 3+1 paradigm [65–67]. However, there exist differences in their results corresponding to the fits in the parameter space $\Delta m_{41}^2 - \sin^2 \theta_{34}$. There is also the difficulty in reconciling the appearance data with the disappearance data. Keeping these points in mind, we adhere to the constraints on 3+1 from the disappearance data from the above-mentioned standalone experiments.

1. The first term is, in its exact form, a rapidly oscillating term due to the large mass-squared difference. In the plots to follow, for specificity, we assume it to be $\simeq 1 \text{ eV}^2$, and adopt the DUNE baseline of 1300 km.
2. Of the three phases, only two linear combinations appear: $\delta_1 = \delta_{13} + \delta_{34}$ and $\delta_2 = \delta_{34} - \delta_{24}$; and only the latter is responsible for CP violation in neutral currents.

It follows that these simplifications and characteristics percolate into $P_{NC} = 1 - P_{\mu s}$, which we now plot in Fig. 2.

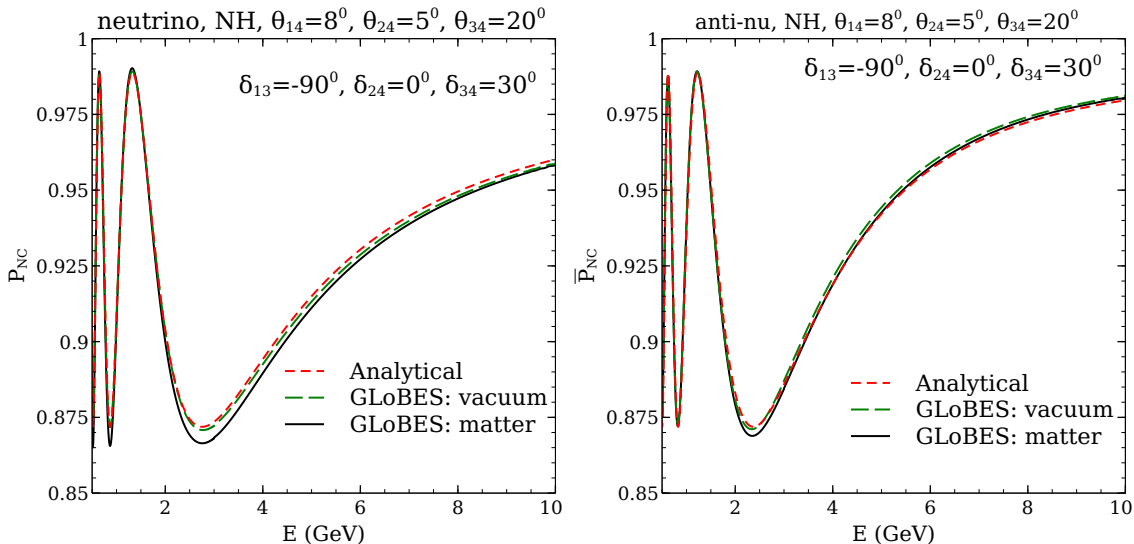


Figure 2: Probability plots, comparing $P_{NC} = 1 - P_{\mu s}$ using the approximate formula for $P_{\mu s}$ given in the text, Eq. 3.2 (red dashed curves) with the full GLoBES result in vacuum (green dashed curves) and matter (black solid curves). The left panel is for neutrinos and the right one for anti-neutrinos. Choices of phases and mixing angles have been made as shown. The curves correspond to $L = 1300 \text{ km}$.

We see that there is good agreement between the exact GLoBES curves (solid black and dashed green lines) and the ones generated by the analytical approximation (red dashed line). The curves show no rapid oscillations since the small wavelength oscillation part of first term in $P_{\mu s}$ is averaged out to 0.5.

From Fig. 2 we see that the approximate formula, derived for the vacuum case, also works well for matter, *i.e.* the overall matter effect in NC event rates is small. Some understanding of this feature can be gleaned from Fig 3, which shows full GLoBES curves for the various probabilities, and demonstrates how the $\nu_\mu \rightarrow \nu_e$ and $\nu_\mu \rightarrow \nu_\tau$ channels have matter effects that are already small in each of these channels, and that nearly cancel each other over the DUNE energy range and baseline. While we certainly cannot generalise this over baselines, energies and new physics scenarios, we note that such a near cancellation can occur for a range of baselines and energies in the 3+0 scenario⁹.

Finally, we note that the NC probabilities for neutrinos and anti-neutrinos are very similar, as a comparison of the left and right panels in Figs. 2 and 3 demonstrate.

⁹For a fuller discussion of the 3+0 case see [68].

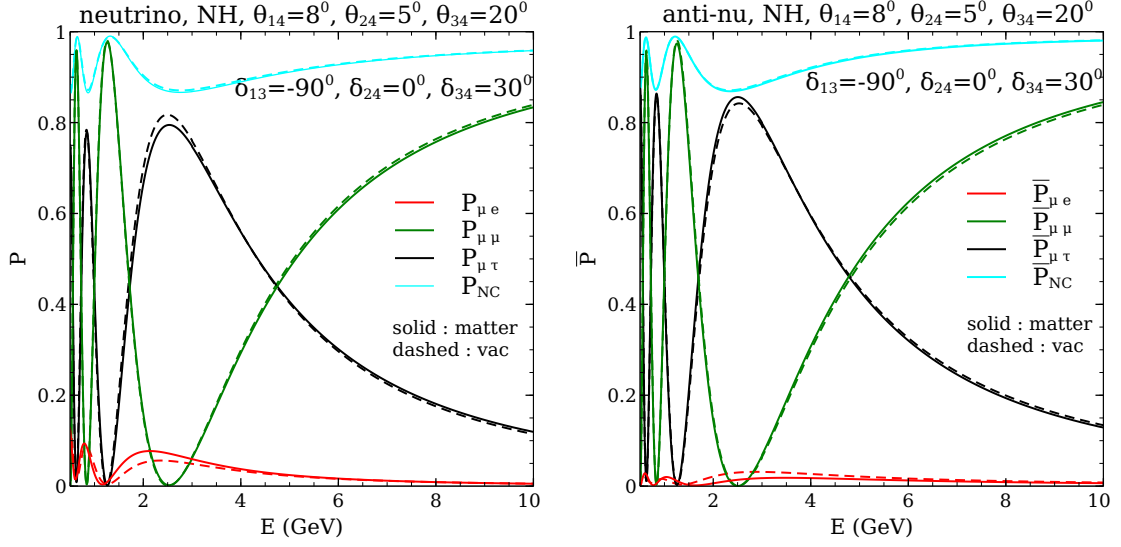


Figure 3: Probability plots, comparing $P_{\mu e}$, $P_{\mu\tau}$, $P_{\mu\mu}$ and $P_{NC} = 1 - P_{\mu s}$, all for the 3+1 model, using GLOBES. The left panel is for neutrinos and the right one for anti-neutrinos, and solid curves are for matter while the dashed ones are for vacuum. Choices of phases and mixing angles have been made as shown. The curves correspond to $L = 1300$ km.

3.2 Effect of the CP violating phases on P_{NC}

This section attempts to understand the dependence of P_{NC} on the three CP violating phases δ_{13} , δ_{24} and δ_{34} in a simple way.

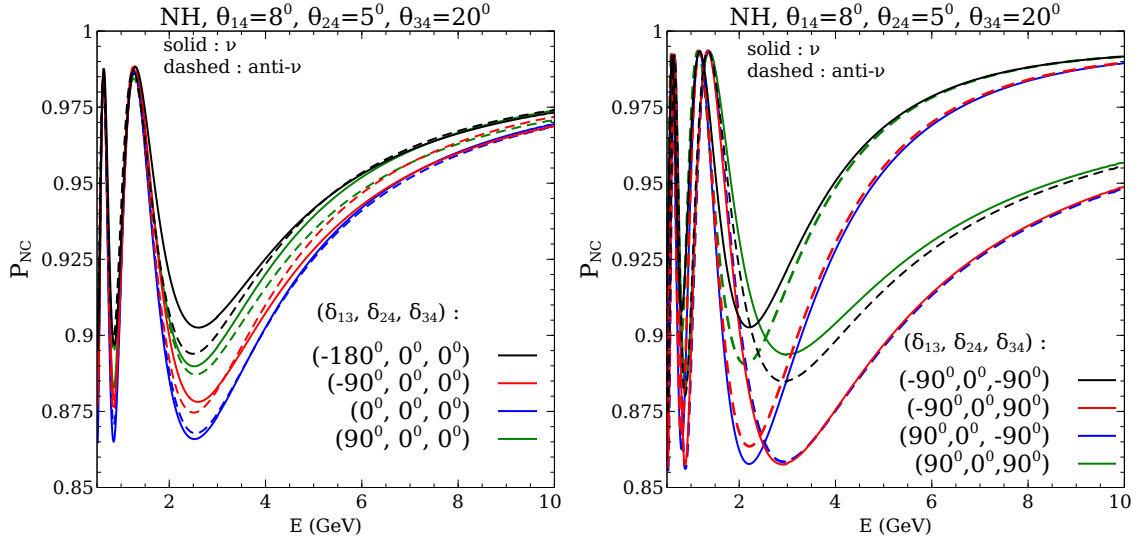


Figure 4: P_{NC} vs Energy (in GeV) assuming normal hierarchy for $L = 1300$ km in the presence of matter. $\theta_{14} = 8^\circ, \theta_{24} = 5^\circ, \theta_{34} = 20^\circ$ (fixed). The solid (dashed) curves are for neutrino (anti-neutrino). Left panel: $\delta_{13} \in \{-180^\circ, -90^\circ, 0^\circ, 90^\circ\}$, $\delta_{24} = \delta_{34} = 0$. Right panel: $\delta_{13}, \delta_{34} \in \{\pm 90^\circ, \pm 90^\circ\}$ and $\delta_{24} = 0$ as shown in the key.

In Fig. 4 we have plotted the $P_{NC} = 1 - P_{\mu s}$ as a function of the Energy (GeV) in the presence of matter for $L = 1300$ km. The plots correspond to normal hierarchy, $\theta_{14} = 8^\circ$, $\theta_{24} = 5^\circ$ and $\theta_{34} = 20^\circ$. The solid curves show the probability values for neutrinos while the dashed ones are for anti-neutrinos. In the left panel we show the dependence of P_{NC} on the δ_{13} phase. For this panel, we show curves corresponding to $\delta_{13} = -180^\circ, -90^\circ, 0$ and 90° . The other two phases δ_{24} and δ_{34} have been set to 0. In the right panel, we show the dependence of P_{NC} on the δ_{13} and δ_{34} phases with the δ_{24} phase kept equal to 0. We show four set of curves for both neutrinos and anti-neutrinos corresponding to $\delta_{13}, \delta_{34} \in \{\pm 90^\circ, \pm 90^\circ\}$. From Fig. 4, we can draw the following conclusions:

- P_{NC} has significant dependence on the CP phases δ_{13} and δ_{34} .
- The left panel shows that the differences between neutrino and anti-neutrino probabilities are small. However, there is appreciable separation between the $\delta_{13} = 0, -180^\circ$ and $\delta_{13} = -90^\circ, 90^\circ$ curves. This can be understood from Eq. 3.2 where the δ_{13} -dependence is through a cosine term.
- In the right panel, the introduction of the δ_{34} phase induces larger differences between the neutrino and anti-neutrino probabilities, specially at higher energies. Referring to Eq. 3.2, we see that as the energy increases, the CP violating term will tend to undergo less suppression compared to the other terms, hence its effect tends to become more visible. Thus, the measurement of a large CP-asymmetry in the NC events at DUNE can point to a CP-violating value of δ_{34} ¹⁰.
- In the right panel, for neutrinos, while the peaks for all curves have about the same value of P_{NC} , among the minima, the lowest value of P_{NC} occurs for $(\delta_{13}, \delta_{34})$ values around $(-90^\circ, 90^\circ)$ while the highest value occurs for $(\delta_{13}, \delta_{34})$ values around $(-90^\circ, -90^\circ)$. For anti-neutrinos, again, examining minima, the lowest value of P_{NC} occurs for $(\delta_{13}, \delta_{34})$ values around $(90^\circ, -90^\circ)$ while the highest value occurs for $(\delta_{13}, \delta_{34})$ values around $(90^\circ, 90^\circ)$. This again, is easy to understand from Eq. 3.2, where the CP dependence is of the form $A \cos(\delta_{13} + \delta_{34}) + B \sin \delta_{34}$ for $\delta_{24} = 0$. Note that here we have shown the curves for restrictive values of δ_{13} and δ_{34} , but this behaviour is verified again in Fig. 6 in a more general way.
- It is also evident from the right panel of Fig. 4 that the probability curve for neutrino corresponding to $(\delta_{13}, \delta_{34})$ of let's say (x, y) where $x, y = \pm 90^\circ$ is degenerate with the anti-neutrino curve of $(-x, -y)$, especially at higher and lower energies. Small differences due to matter effects can be seen near the minima. Neglecting these small matter effects, we see from the approximate expression for the vacuum oscillation probability, Eq. 3.2, that the degenerate probability curves should indeed be identical.

Under the approximations in which Eq. 3.2 is valid, it can be seen that there are only two effective CP phases that will play a role in P_{NC} at the leading order. These are $\delta_1 = \delta_{13} + \delta_{34}$ and $\delta_2 = \delta_{34} - \delta_{24}$. Thus, in our chosen parameterisation of the PMNS

¹⁰Or, more accurately, a CP-violating value of $\delta_2 = \delta_{34} - \delta_{24}$, as we emphasise below.

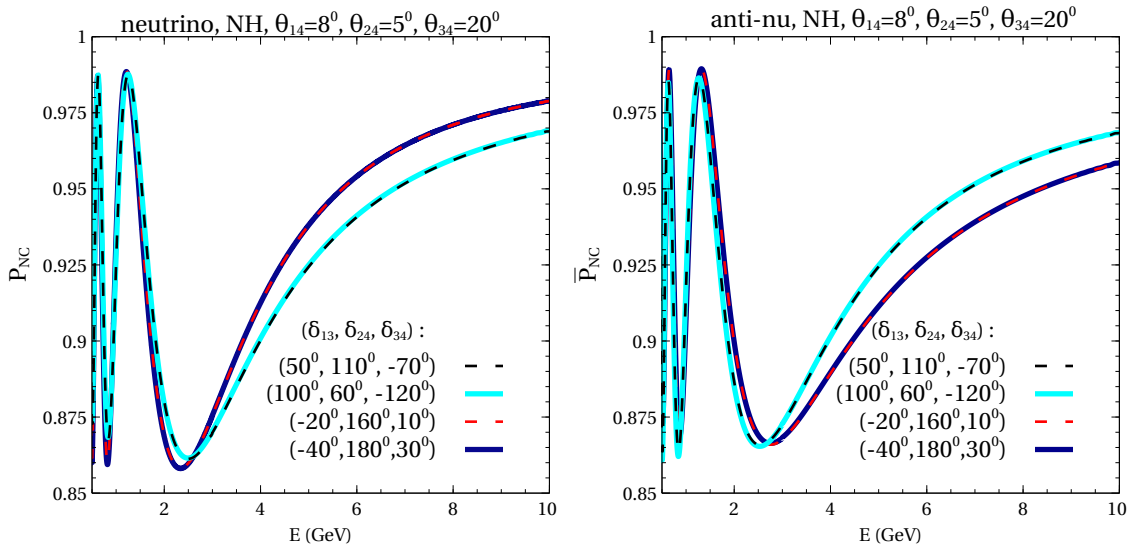


Figure 5: P_{NC} vs Energy (in GeV) assuming normal hierarchy for $L = 1300$ km in the presence of matter. $\theta_{14} = 8^\circ$, $\theta_{24} = 5^\circ$, $\theta_{34} = 20^\circ$ (fixed). The left (right) panel corresponds to neutrino (anti-neutrino) probabilities. Different values of δ_{13} , δ_{24} , δ_{34} are chosen as shown in the key.

matrix, there is a degeneracy between the three CP phases. We show this explicitly in Fig. 5. We have plotted P_{NC} as a function of the energy for neutrinos (anti-neutrinos) in the left (right) panel. We choose two sets of different $(\delta_{13}, \delta_{24}, \delta_{34})$ values (as shown in the key in the figures) which give the same δ_1 and δ_2 values. The assumed values of the other oscillation parameters are same as Fig. 4. It can be seen that there is almost complete degeneracy between the curves corresponding to common values of the phases δ_1 and δ_2 . Note that Eq. 3.2 is derived for vacuum, and for the special value $\theta_{23} = 45^\circ$. However the degeneracies hold true for matter probabilities at $L = 1300$ km and for other assumed values of θ_{23} within its allowed range.

It is therefore possible to set one of the phases equal to 0, without the loss of generality. Since, we have considered $\sin\theta_{24}$ to be a small quantity as its range of values is the most restricted, putting $\delta_{24} = 0$ may be the best choice in order to not have significant differences between vacuum and matter probabilities. We explore this in Fig. 6, generated using GLoBES. These plots show the values of probabilities in the $P_{NC} - \bar{P}_{NC}$ plane for different values of the oscillation parameters. In Fig. 6, we show results for normal hierarchy, $\theta_{14} = 8^\circ$, $\theta_{24} = 5^\circ$ and $\theta_{34} = 20^\circ$. The left (right) panel corresponds to neutrino energy of 3 GeV (5 GeV). The green region shows the space in the $P_{NC} - \bar{P}_{NC}$ plane when all the three phases are varied in the range $[-180^\circ, 180^\circ]$. The red region corresponds to the space when δ_{13} and δ_{34} are varied in $[-180^\circ, 180^\circ]$, holding δ_{24} equal to 0. The four black points correspond to $\delta_{13}, \delta_{34} \in \{\pm 90^\circ, \pm 90^\circ\}$ when $\delta_{24} = 0$. From Fig. 6, we conclude that

- The fact that the red region is almost the same as the green region suggests that putting $\delta_{24} = 0$ does not lead to any loss of obtainable $P_{NC} - \bar{P}_{NC}$ space.
- The four black points - $\delta_{13}, \delta_{34} \in \{\pm 90^\circ, \pm 90^\circ\}$ indeed quite closely correspond to

the δ_{13}, δ_{34} values for which the the P_{NC} and \bar{P}_{NC} are minimum or maximum. This is true for both 3 GeV and 5 GeV.

- The dependence on the δ_{13} and δ_{34} phases as expressed in Eq. 3.2 is reasonably accurate.

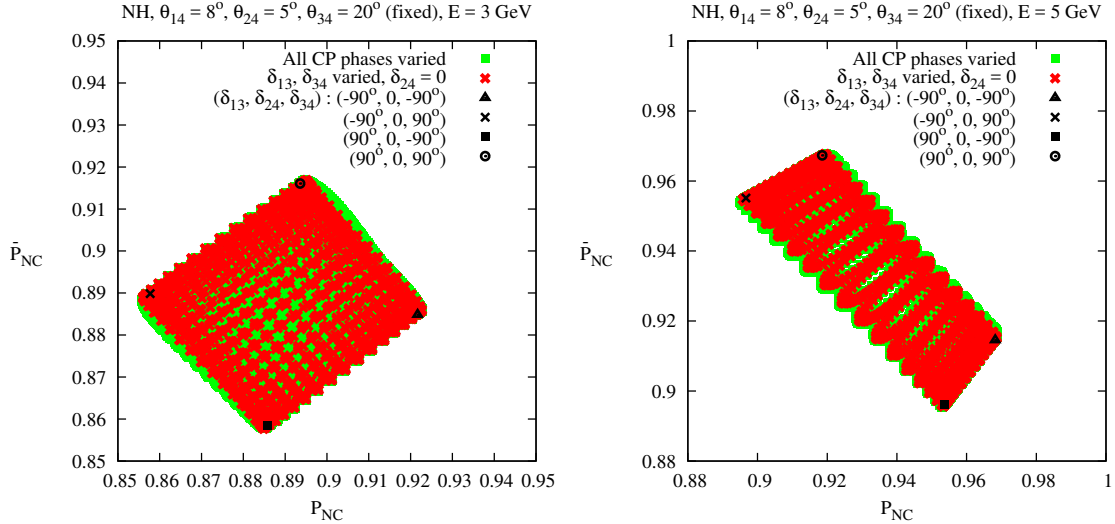


Figure 6: \bar{P}_{NC} vs P_{NC} at $E = 3$ GeV (left-panel) and at $E = 5$ GeV (right-panel) for $L = 1300$ km in the presence of matter. $\theta_{14} = 8^\circ, \theta_{24} = 5^\circ, \theta_{34} = 20^\circ$ (fixed). Green region: This region corresponds to all $\bar{P}_{NC} - P_{NC}$ values that are obtained when all the three CP phases are varied in $[-180^\circ, 180^\circ]$. Red region: This region corresponds to all $\bar{P}_{NC} - P_{NC}$ values that are obtained when δ_{13} and δ_{34} are varied in $[-180^\circ, 180^\circ]$ while $\delta_{24} = 0$. Black points: $\delta_{13}, \delta_{34} \in \{\pm 90^\circ, \pm 90^\circ\}$ when $\delta_{24} = 0$.

Finally, we point out that the situation above serves as another example of the point made in Section 2. The NC events for the long baseline of DUNE and the chosen 3+1 new physics scenario provide a window into CP via the phase combinations $\delta_1 = \delta_{13} + \delta_{34}$ and $\delta_2 = \delta_{34} - \delta_{24}$ both in vacuum and in matter. On the other hand, as discussed in [11], the CC probability $P_{\mu e}$ in matter for the same scenario is sensitive to all three CP phases¹¹, which leads to degeneracies. Thus NC measurements, with their high statistics, are an important complementary tool to probe CP and break degeneracies in new physics scenarios in conjunction with CC measurements.

4 Neutral current measurements as a tool to break BSM physics degeneracies

In this section, we demonstrate the capability of NC events to break degeneracies which would otherwise arise in CC events, vis a vis new physics scenarios. While we choose propagation based non-standard interactions (NSI) and a 3+1 sterile scenario to demonstrate our point, our conclusion will hold for any two new physics settings, one of which does not

¹¹In vacuum, as discussed in [11], the CC probability has no sensitivity to δ_{34} .

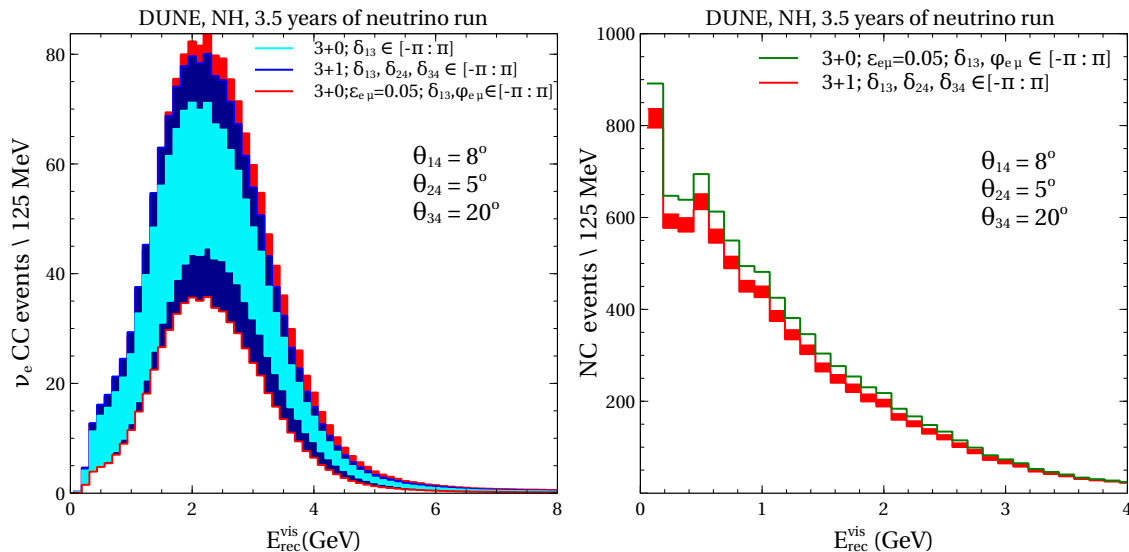


Figure 7: CC and NC events as a function of reconstructed neutrino energy in DUNE with 3.5 yrs of neutrino running. The left panel corresponds to ν_e CC events for two different new physics scenarios, as well as for the standard 3+0 paradigm. The green line and the red band in the right panel show NC neutrino events in the presence of propagation-related NSI, and in the presence of a sterile neutrino, respectively. In all cases the respective CP phases have been varied over their full range of $[-180^\circ, +180^\circ]$. In the case of NSIs, $A(\delta_{e\alpha}\delta_{e\beta} + \epsilon_{\alpha\beta}e^{i\phi_{\alpha\beta}})$ ($\alpha, \beta = e, \mu, \tau$) represents the matter term in the effective Hamiltonian in the presence of NSIs. Here, A is the Wolfenstein matter term and is given by $A(\text{eV}^2) = 0.76 \times 10^{-4} \rho(\text{g/cc})E(\text{GeV})$, ρ being the matter density and E , the neutrino energy. The chosen example values of NSI and sterile parameters are shown in the key. The remaining NSI parameters are equal to 0.

break 3+0 unitarity (in this example, the propagation NSI) and another one which does (3+1 sterile). A similar conclusion would hold, for example, for NSI in propagation and neutrino decay, or NSI in propagation and NSI in production or detection (which inherently violate unitarity by adding to or depleting the source neutrino beam).

Both NSI arising during propagation and extra sterile neutrino states affect ν_e CC events. From Fig. 7 (left panel) we see that there is a wide range of possible spectra that can arise either from propagation NSI or an extra sterile neutrino state (3+1 scenario). Shown also is the standard 3+0 scenario band. NSI affect the individual transition probabilities but the total oscillation probability of all the active flavours remains unity. On the other hand, in the presence of extra sterile states, the total oscillation probability of the active flavours becomes less than unity, leading to a depletion in NC events in the presence of sterile states compared to propagation NSI (the right panel of Fig. 7). Thus, NC events break the degeneracy seen in the CC event spectrum. We expect around 9345 NC total signal events in the case of 3+0 (or with propagation NSI present) in DUNE for 3.5 years of neutrino run. With 3+1 and sterile oscillation parameters corresponding to the right panel of Fig. 7, this number will deplete to $\sim (8306 - 8804)$ depending on the true values of the CP violating phases. Thus, a 6% - 11% reduction in the total NC signal event rate is possible for $\theta_{34} \approx 20^\circ$. We do quantitative analyses in Sec. 5, to show that with a reduction in NC rates of this size, DUNE can distinguish between the 3+0 (or propagation

NSI) and the 3+1 scenarios at a 90% C.L.

We note that as the sterile parameters become small, the 3+1 and 3+0 scenarios merge and become indistinguishable. In other words, the red band in the right panel of Fig. 7 will tend to grow narrower and merge with the green solid line. Thus, the 3+1 parameters need to be such that a measurable difference in the NC rate can be attained.

5 Constraints on the 3+1 paradigm: Sensitivity forecasts with DUNE

In this section, we demonstrate the sensitivity of the DUNE experiment to exclude the 3+1 scenario using a combined analysis of NC and CC measurements. We assume a 40 kt Liquid Argon detector and 3.5 years each of neutrino and anti-neutrino running. We have used the optimised beam profile, as described earlier in Section 3. The CC and NC events due to such a beam have been shown in Figs. 1 and 7. We simulate data assuming that 3+0 is the true case i.e. we put the mixing parameters $\Delta m_{41}^2, \theta_{14}, \theta_{24}, \theta_{34}, \delta_{24}$ and δ_{34} equal to 0. Note that in such a situation δ_{13} is δ_{CP} . We assume the hierarchy to be normal, $\theta_{12} = 33.48^\circ$, $\theta_{13} = 8.5^\circ$ and $\theta_{23} = 45^\circ$. The mass-squared differences Δm_{21}^2 and $|\Delta m_{31}^2|$ have been taken to be $7.5 \times 10^{-5} \text{eV}^2$ and $2.45 \times 10^{-3} \text{eV}^2$ [69–71] respectively. The CP phase δ_{13} is assumed to be -90° , based on the recent hints from [72, 73]. We now fit this simulated data with events generated assuming the 3+1 scenario. We consider $\theta_{14} \in [0, 12^\circ]$ ¹², $\theta_{34} \in [0, 50^\circ]$ ¹³, $\theta_{23} \in [40^\circ, 50^\circ]$, δ_{13} and $\delta_{34} \in [-180^\circ, +180^\circ]$ and $\Delta m_{41}^2 \in [0.1, 10] \text{eV}^2$. Previously, we argued that the results with NC data will not depend significantly on the parameters θ_{24} and δ_{24} . However, the same is not true of the CC events i.e. the $\nu_\mu \rightarrow \nu_e$ and $\nu_\mu \rightarrow \nu_\mu$ oscillation channels. Hence, in the fit, we vary $\theta_{24} \in [0, 4^\circ]$ ¹⁴ and $\delta_{24} \in [-180^\circ, +180^\circ]$. We assume the hierarchy to be known and hence do not consider the inverted hierarchy while fitting. We generate event spectra for various combinations of these 3+1 test oscillation parameters and then calculate the binned Poissonian $\Delta\chi^2$ between such test events spectra and the simulated 3+0 true events spectra (data). We have assumed 5% normalisation error for the signal events and 10% normalisation error for the background events. The $\Delta\chi^2$ are marginalised over these systematic uncertainties through the method of pulls.

In Fig. 8, we show the sensitivity of the DUNE experiment to exclude the 3+1 paradigm with NC and CC measurements. *We consider the test case of $\Delta m_{41}^2 = 1 \text{eV}^2$.* In producing these plots, we have not considered the variation of the CP violating phases in the fit, so as to show the effect of the mixing angles only. That is, we show the results corresponding to test $(\delta_{13}, \delta_{24}, \delta_{34}) = (-90^\circ, 0, 0)$. We show the 90% C.L. limits (corresponding to $\Delta\chi^2 = 4.61$ for a two-parameter fit) in the test θ_{14} - test θ_{34} plane for different values of test θ_{24} . The left panel in Fig. 8 corresponds to the choice of test $\theta_{24} = 0$ and the right panel corresponds to test $\theta_{24} = 4^\circ$, as depicted in the figure titles. We show results for NC stand-alone data, appearance stand-alone data, disappearance stand-alone data, appearance and disappearance combined (i.e. CC data) and finally all data i.e. CC and

¹²The 90% C.L. allowed range for θ_{14} has been taken from [59].

¹³Note that, the allowed range of θ_{34} from [63] is $\theta_{34} \in [0, 23^\circ]$ at 90% C.L. However, in order to show the individual contributions from various channels we consider larger values of θ_{34} .

¹⁴The results from IceCube [60] dictate the allowed range for θ_{24} at 90% C.L.

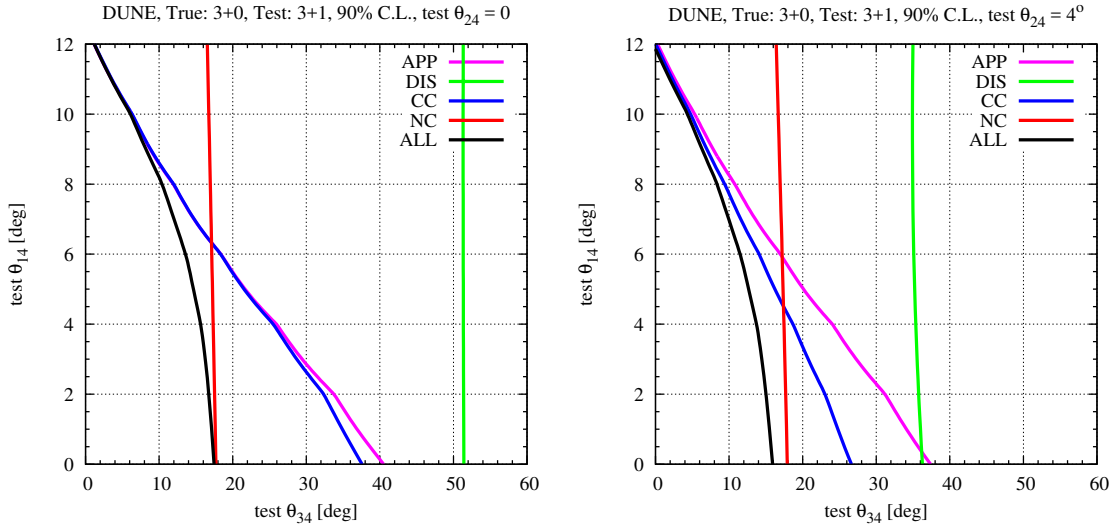


Figure 8: 90% ($\Delta\chi^2 = 4.61$) C.L. contour plots in the test θ_{14} - test θ_{34} plane for different choices of test θ_{24} . Left: test $\theta_{24} = 0$ and Right: test $\theta_{24} = 4^\circ$. The true case has been taken to be 3+0 and the test case is 3+1. The value of test Δm_{41}^2 is 1eV^2 for both the plots. The results are for the DUNE experiment with 3.5 years each of neutrino and anti-neutrino running. For these figures, test $(\delta_{13}, \delta_{24}, \delta_{34}) = (-90^\circ, 0, 0)$ i.e. the $\Delta\chi^2$ has not been marginalised over the test CP phases. We show results for the NC standalone data, appearance standalone data, disappearance standalone data, appearance and disappearance data combined (CC) and finally, the CC and the NC data combined (“ALL”).

NC combined. This helps to better understand the contribution that each type of data has in excluding the 3+1 scenario with respect to the given active-sterile mixing angle. The regions that lie towards the increasing values of test θ_{14} and test θ_{34} are the ones for which DUNE can exclude 3+1 at 90% C.L. An examination of the Fig. 8 allows us to draw some important conclusions:

- The NC data by itself constrains mainly the θ_{34} angle and this constraint has a small dependence on the test values of the mixing angles θ_{14} and θ_{24} . The most conservative exclusion of the θ_{34} angle corresponds to $\theta_{14} = 0$ where $\theta_{34} \gtrsim 18^\circ$ is excluded by the data. The strongest bound of $\theta_{34} \gtrsim 16^\circ$ corresponds to $\theta_{14} = 12^\circ$.
- The appearance data are sensitive to all three active-sterile mixing angles. At $\theta_{34} = 0$, $\theta_{14} \lesssim 12^\circ$ is allowed for both $\theta_{24} = 0$ and $\theta_{24} = 4^\circ$. However, the constraints on θ_{34} are somewhat weak and strongly-correlated with the values of test θ_{14} . The weakest constraints are obtained for $\theta_{14} = 0$, which excludes values corresponding to $\theta_{34} \gtrsim 38^\circ$.
- The disappearance data are mainly sensitive to θ_{24} and θ_{34} . The constraints are essentially independent of the value of test θ_{14} . The strongest constraint, of $\theta_{34} \gtrsim 36^\circ$ being ruled-out, occurs when test $\theta_{24} = 4^\circ$.
- The combined NC+CC data are quite sensitive to θ_{34} . If $\theta_{24} = 4^\circ$ and $\theta_{14} \sim 0$, then

$\theta_{34} \gtrsim 16^\circ$ can be ruled out. For $\theta_{24} = 4^\circ$ and $\theta_{14} \sim 12^\circ$, DUNE data can rule out $\theta_{34} \gtrsim 0$.

It is quite evident from the above discussions that the NC data have a marked advantage over the CC data in excluding the 3+1 paradigm when the mixing angles θ_{14} and θ_{24} are very small. If it so happens that the angles θ_{14} and θ_{24} are small but the angle θ_{34} is large, then, even though the appearance and the disappearance data would not show any hints of new physics, there would be a clear evidence of new physics in the NC data.

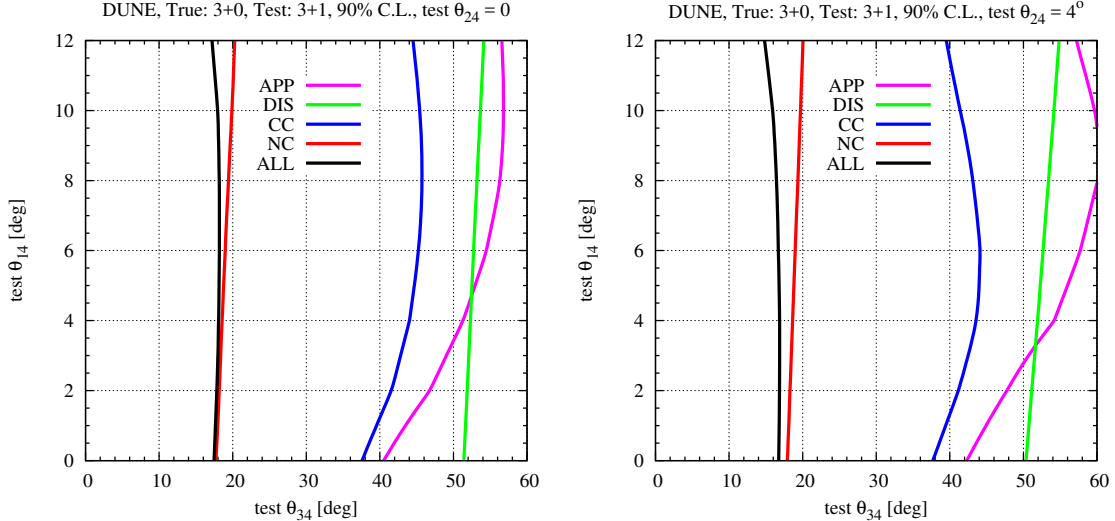


Figure 9: 90% ($\Delta\chi^2 = 4.61$) C.L. contour plots in the test θ_{14} - test θ_{34} plane for different choices of test θ_{24} . Left: test $\theta_{24} = 0$ and Right: test $\theta_{24} = 4^\circ$. The true case has been taken to be 3+0 and the test case is 3+1. The value of test Δm_{41}^2 is 1eV^2 for both the plots. The results are for the DUNE experiment with 3.5 years each of neutrino and anti-neutrino running. For these figures, the $\Delta\chi^2$ has been marginalised over the test CP phases. We show results for the NC standalone data, appearance standalone data, disappearance standalone data, appearance and disappearance data combined (CC) and finally, the CC and the NC data combined (“ALL”).

In obtaining Fig. 8, effects of the three CP phases were not taken into account and each of the three of them were held fixed at their input true values. In Fig. 9, we repeat the same exercise as that in Fig. 8, except that, for each test combination of values of θ_{14}, θ_{24} and θ_{34} , we marginalise the $\Delta\chi^2$ over the three CP phases δ_{13}, δ_{24} and δ_{34} and select the smallest $\Delta\chi^2$. Thus, Fig. 9 correctly takes into account the lack of knowledge regarding the CP violating phases. It can be seen that the results due to CC appearance are significantly affected because of marginalisation over the CP phases. This physics point was emphasised in [11, 27]. While for the plots in Fig. 8, a significant region of the given $\theta_{14} - \theta_{34}$ parameter space was ruled out by the appearance data; for the plots in Fig. 9, most of such $\theta_{14} - \theta_{34}$ region is allowed at 90% C.L. This holds true especially at the larger values of θ_{14} . Thus, with CC data alone, DUNE cannot be expected to provide significant constraints on θ_{34} . On the other hand, the effect of marginalisation over CP phases on the NC data is small. Thus, NC data can decisively constrain the mixing angle θ_{34} even when

the CP phases are unknown, as can be seen in the plots in Fig. 9. Therefore, another advantage that the NC events have over CC is that they are more immune to the lack of knowledge regarding the CP phases. *Even with CP violating phases present, it would be easier to rule out a moderately large value of θ_{34} with the NC data compared to ruling out moderately large values of θ_{14} and θ_{24} with the CC data.* Taking into account the marginalisation over all the relevant mixing angles and the CP phases, the combined NC and CC data from DUNE can exclude the 3+1 paradigm for $\theta_{34} \gtrsim 18^\circ$. With reference to Fig. 8 and Fig. 9, we note that in Fig. 8, the most conservative estimate of θ_{34} corresponds to $\theta_{14} = 0$. This is no longer true in Fig. 9 where the most conservative constraints on θ_{34} occur at larger values of θ_{14} . This difference is stark in the case of CC data which reinforces the importance of CP phases in the CC channels. For NC too, this argument holds true although the differences are much smaller in nature.

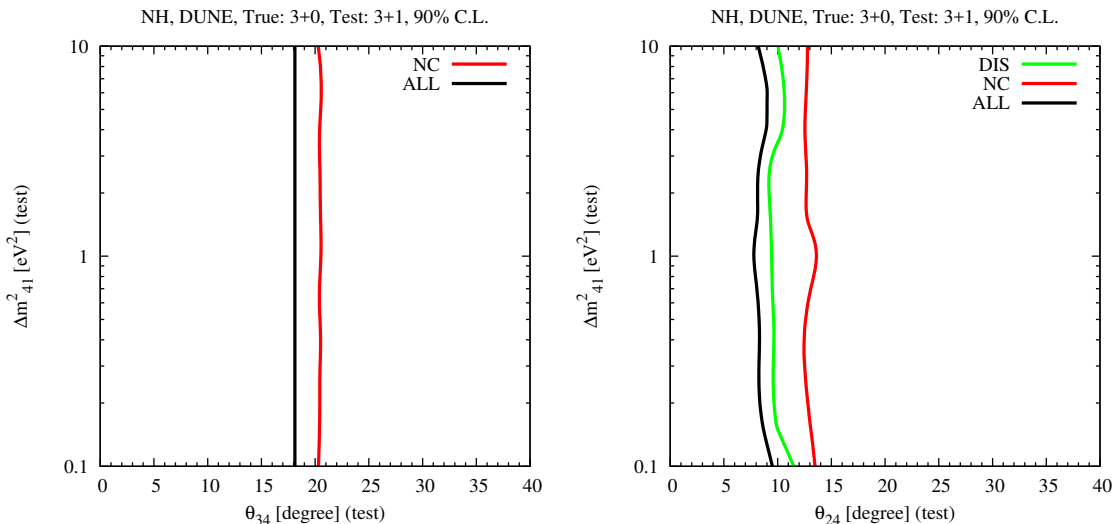


Figure 10: 90% ($\Delta\chi^2 = 4.61$) C.L. contour plots for 3+1 exclusion in the test Δm_{41}^2 - test θ_{34} space (left) and test Δm_{41}^2 - test θ_{24} space (right). The results are for the DUNE experiment with 3.5 years each of neutrino and anti-neutrino running. The true case has been taken to be 3+0 and the test to be 3+1. In the left panel, we show results with the NC data, and NC and CC data combined (“ALL”). In the right panel, we show results with the NC data, the disappearance data (“DIS”) and the NC and CC data combined (“ALL”).

To show how the exclusion of the 3+1 paradigm depends on the mass-squared difference Δm_{41}^2 , we repeat the exercise done in Fig. 8 for test Δm_{41}^2 values ranging in $[0.1, 10]$ eV^2 . We marginalise over the two mixing angles θ_{14} and θ_{24} , in addition to the CP phases, and report the minimum $\Delta\chi^2$ as a function of test Δm_{41}^2 and test θ_{34} . The results are shown in the left panel of Fig. 10. Note that the other details regarding the simulation and assumptions on the oscillation parameters remain the same as those in Fig. 8. It is easy to see that the results do not depend much on the mass-squared difference Δm_{41}^2 . At 90% C.L., $\theta_{34} \gtrsim 18^\circ$ can be ruled out with the combined CC and NC data. With NC data alone, $\theta_{34} \gtrsim 20^\circ$ can be ruled out at 90% C.L. NC data is most effective in constraining

θ_{34} . On combining the NC data with the CC data an improvement of $\approx 2^\circ$ is seen.

We show DUNE's ability to constrain the $\Delta m_{41}^2 - \theta_{24}$ parameter space in the right panel of Fig. 10. We consider test Δm_{41}^2 values ranging in $[0.1, 10]$ eV^2 and test θ_{24} values in $[0, 40^\circ]$. In the fit, we marginalise over θ_{14} and θ_{34} and the three CP violating phases. It can be seen that most of the sensitivity to the exclusion of θ_{24} comes from the disappearance data. With the CC and NC data combined, DUNE can rule out $\theta_{24} \gtrsim 9^\circ \pm 1^\circ$ depending on the test value of Δm_{41}^2 . The current results from IceCube already exclude $\theta_{24} \gtrsim 4^\circ$ at 90% C.L. for test $\Delta m_{41}^2 \approx 0.5 \text{ eV}^2$. However, IceCube's θ_{34} -constraint is strongly correlated with the test value of Δm_{41}^2 and it can be seen in [60] that for test $\Delta m_{41}^2 \approx 10 \text{ eV}^2$, the constraints from the IceCube data worsen to $\theta_{24} \gtrsim 45^\circ$ at 90% C.L. DUNE, on the other hand, can provide a strong constraint on θ_{24} that is relatively independent of test Δm_{41}^2 .

6 Summary and concluding remarks

This work attempts to examine how NC events can synergistically aid the search for new physics and CP violation when combined with other measurements. We show that typically the NC events offer a window to CP phases and mixing angles that is complementary to that accessed by CC event measurements at both long and short baseline experiments. They can break degeneracies existing in CC measurements, allowing one to distinguish between new physics that violates 3+0 unitarity and new physics that does not. NC events seem not to be affected greatly by matter effects which arise at energies and baselines relevant to DUNE, rendering analytical understanding of new physics somewhat easier. They also aid in constraining parameters that are not easily accessible to CC measurements. Overall, in an experimental era when combined measurements can lead to significantly increased precision and understanding, NC studies can play a valuable role in the search for new physics at neutrino detectors.

Acknowledgements

We are grateful to Michel Sorel for providing us with the migration matrices used in this work, for a calculation probing a feature of the results obtained with these matrices, and for very helpful discussions. RG and BK thank Georgia Karagiorgi and Stephen Parke for very useful conversations, and Mark Ross-Lonergan for some very helpful checks of calculations of Long Baseline oscillation probabilities in 3+1. RG acknowledges support in the form of a Neutrino Physics Center Fellowship from the Neutrino Division and Theory Group at Fermilab. He, SP and SR also acknowledge support from the XII Plan Neutrino Project of the Department of Atomic Energy and the High Performance Cluster Facility at HRI. SP thanks São Paulo Research Foundation (FAPESP) for the support through Funding Grants No. 2014/19164-6 and No. 2017/02361-1. He also thanks RG for the academic visit at Harish-Chandra Research Institute during 2016 - 2017. This research was supported in part by the National Science Foundation under Grant No. NSF PHY11-25915. This manuscript has been authored by Fermi Research Alliance, LLC under Contract No. DE-AC02-07CH11359 with the U.S. Department of Energy, Office of Science, Office of High

Energy Physics. The United States Government retains and the publisher, by accepting the article for publication, acknowledges that the United States Government retains a non-exclusive, paid-up, irrevocable, world-wide license to publish or reproduce the published form of this manuscript, or allow others to do so, for United States Government purposes.

References

- [1] J. Cao et al. (2017), [1704.08181](#).
- [2] A. Sousa, *talk at WIN2017*, URL <https://indico.fnal.gov/contributionDisplay.py?contribId=101&confId=9942>.
- [3] W. Winter, *talk at WIN2017*, URL <https://indico.fnal.gov/contributionDisplay.py?contribId=76&confId=9942>.
- [4] A. Esmaili, F. Halzen, and O. L. G. Peres, JCAP **1307**, 048 (2013), [1303.3294](#).
- [5] A. Chatterjee, P. Mehta, D. Choudhury, and R. Gandhi, Phys. Rev. **D93**, 093017 (2016), [1409.8472](#).
- [6] N. Klop and A. Palazzo, Phys. Rev. **D91**, 073017 (2015), [1412.7524](#).
- [7] S. Choubey, A. Ghosh, T. Ohlsson, and D. Tiwari, JHEP **12**, 126 (2015), [1507.02211](#).
- [8] M. Blennow, S. Choubey, T. Ohlsson, and S. K. Raut, JHEP **09**, 096 (2015), [1507.02868](#).
- [9] J. M. Berryman, A. de Gouvea, K. J. Kelly, and A. Kobach, Phys. Rev. **D92**, 073012 (2015), [1507.03986](#).
- [10] S. Parke and M. Ross-Lonergan, Phys. Rev. **D93**, 113009 (2016), [1508.05095](#).
- [11] R. Gandhi, B. Kayser, M. Masud, and S. Prakash, JHEP **11**, 039 (2015), [1508.06275](#).
- [12] A. de Gouvea and K. J. Kelly, Nucl. Phys. **B908**, 318 (2016), [1511.05562](#).
- [13] P. Coloma, JHEP **03**, 016 (2016), [1511.06357](#).
- [14] D. V. Forero and P. Huber, Phys. Rev. Lett. **117**, 031801 (2016), [1601.03736](#).
- [15] J. Liao and D. Marfatia, Phys. Rev. Lett. **117**, 071802 (2016), [1602.08766](#).
- [16] J. M. Berryman, A. de Gouvea, K. J. Kelly, O. L. G. Peres, and Z. Tabrizi, Phys. Rev. **D94**, 033006 (2016), [1603.00018](#).
- [17] M. Masud and P. Mehta, Phys. Rev. **D94**, 013014 (2016), [1603.01380](#).
- [18] S. K. Agarwalla, S. S. Chatterjee, and A. Palazzo, JHEP **09**, 016 (2016), [1603.03759](#).
- [19] S. Choubey and D. Pramanik, Phys. Lett. **B764**, 135 (2017), [1604.04731](#).
- [20] O. G. Miranda, M. Tortola, and J. W. F. Valle, Phys. Rev. Lett. **117**, 061804 (2016), [1604.05690](#).
- [21] P. Coloma and T. Schwetz, Phys. Rev. **D94**, 055005 (2016), [Erratum: Phys. Rev. **D95**, no.7,079903(2017)], [1604.05772](#).
- [22] S.-F. Ge, P. Pasquini, M. Tortola, and J. W. F. Valle, Phys. Rev. **D95**, 033005 (2017), [1605.01670](#).
- [23] S. K. Agarwalla, S. S. Chatterjee, and A. Palazzo, Phys. Rev. Lett. **118**, 031804 (2017), [1605.04299](#).

- [24] M. Masud and P. Mehta, Phys. Rev. **D94**, 053007 (2016), [1606.05662](#).
- [25] M. Blennow, S. Choubey, T. Ohlsson, D. Pramanik, and S. K. Raut, JHEP **08**, 090 (2016), [1606.08851](#).
- [26] S. K. Agarwalla, S. S. Chatterjee, and A. Palazzo, Phys. Lett. **B762**, 64 (2016), [1607.01745](#).
- [27] D. Dutta, R. Gandhi, B. Kayser, M. Masud, and S. Prakash, JHEP **11**, 122 (2016), [1607.02152](#).
- [28] S. Verma and S. Bhardwaj (2016), [1609.06412](#).
- [29] D. Dutta, P. Ghoshal, and S. Roy, Nucl. Phys. **B920**, 385 (2017), [1609.07094](#).
- [30] M. Blennow, P. Coloma, E. Fernandez-Martinez, J. Hernandez-Garcia, and J. Lopez-Pavon, JHEP **04**, 153 (2017), [1609.08637](#).
- [31] D. Dutta, P. Ghoshal, and S. K. Sehrawat, Phys. Rev. **D95**, 095007 (2017), [1610.07203](#).
- [32] F. J. Escrihuela, D. V. Forero, O. G. Miranda, M. Trtola, and J. W. F. Valle (2016), [1612.07377](#).
- [33] K. N. Deepthi, S. Goswami, and N. Nath (2016), [1612.00784](#).
- [34] D. Cianci, A. Furmanski, G. Karagiorgi, and M. Ross-Lonergan (2017), [1702.01758](#).
- [35] J. Rout, M. Masud, and P. Mehta, Phys. Rev. **D95**, 075035 (2017), [1702.02163](#).
- [36] S. Choubey, D. Dutta, and D. Pramanik (2017), [1704.07269](#).
- [37] M. Masud, M. Bishai, and P. Mehta (2017), [1704.08650](#).
- [38] M. Ghosh, S. Gupta, Z. M. Matthews, P. Sharma, and A. G. Williams (2017), [1704.04771](#).
- [39] S. Choubey, S. Goswami, and D. Pramanik (2017), [1705.05820](#).
- [40] P. Coloma and O. L. G. Peres (2017), [1705.03599](#).
- [41] P. Coloma, D. V. Forero, and S. J. Parke (2017), [1707.05348](#).
- [42] P. Huber, M. Lindner, and W. Winter, Comput.Phys.Commun. **167**, 195 (2005), [hep-ph/0407333](#).
- [43] P. Huber, J. Kopp, M. Lindner, M. Rolinec, and W. Winter, Comput. Phys. Commun. **177**, 432 (2007), [hep-ph/0701187](#).
- [44] J. Kopp, Sterile neutrinos and non-standard neutrino interactions in GLOBES, November 2010. <https://www.mpi-hd.mpg.de/personalhomes/globes/tools/snu-1.0.pdf> (2010).
- [45] J. Kopp, M. Lindner, T. Ota, and J. Sato, Phys. Rev. **D77**, 013007 (2008), [0708.0152](#).
- [46] R. Acciarri et al. (DUNE) (2015), [1512.06148](#).
- [47] L. Camilleri, AIP Conference Proceedings **1680**, 020004 (2015), URL <http://scitation.aip.org/content/aip/proceeding/aipcp/10.1063/1.4931863>.
- [48] M. Antonello et al. (LAr1-ND, ICARUS-WA104, MicroBooNE) (2015), [1503.01520](#).
- [49] A. Aguilar-Arevalo et al. (LSND), Phys. Rev. **D64**, 112007 (2001), [hep-ex/0104049](#).
- [50] A. A. Aguilar-Arevalo et al. (MiniBooNE), Phys. Rev. Lett. **102**, 101802 (2009), [0812.2243](#).
- [51] G. Mention, M. Fechner, T. Lasserre, T. A. Mueller, D. Lhuillier, M. Cribier, and A. Letourneau, Phys. Rev. **D83**, 073006 (2011), [1101.2755](#).
- [52] T. A. Mueller et al., Phys. Rev. **C83**, 054615 (2011), [1101.2663](#).

- [53] A. A. Aguilar-Arevalo et al. (MiniBooNE), Phys. Rev. Lett. **110**, 161801 (2013), [1303.2588](#).
- [54] T. Alion et al. (DUNE) (2016), [1606.09550](#).
- [55] C. Adams et al. (LBNE), in *LBNE* (2013), [1307.7335](#), URL <http://www.osti.gov/scitech/biblio/1128102>.
- [56] V. De Romeri, E. Fernandez-Martinez, and M. Sorel, JHEP **09**, 030 (2016), [1607.00293](#).
- [57] Michel Sorel, Private Correspondence (2017).
- [58] T. J. Carroll, in *52nd Rencontres de Moriond on EW Interactions and Unified Theories (Moriond EW 2017) La Thuile, Italy, March 18-25, 2017* (2017), [1705.05064](#), URL <https://inspirehep.net/record/1599558/files/arXiv:1705.05064.pdf>.
- [59] P. Adamson et al. (MINOS, Daya Bay), Phys. Rev. Lett. **117**, 151801 (2016), [Addendum: Phys. Rev. Lett.117,no.20,209901(2016)], [1607.01177](#).
- [60] M. G. Aartsen et al. (IceCube), Phys. Rev. Lett. **117**, 071801 (2016), [1605.01990](#).
- [61] K. Abe et al. (Super-Kamiokande), Phys. Rev. **D91**, 052019 (2015), [1410.2008](#).
- [62] P. Adamson et al. (MINOS), Phys. Rev. Lett. **117**, 151803 (2016), [1607.01176](#).
- [63] M. G. Aartsen et al. (IceCube), Phys. Rev. **D95**, 112002 (2017), [1702.05160](#).
- [64] P. Adamson et al. (NOvA) (2017), [1706.04592](#).
- [65] J. Kopp, P. A. N. Machado, M. Maltoni, and T. Schwetz, JHEP **05**, 050 (2013), [1303.3011](#).
- [66] G. H. Collin, C. A. Argelles, J. M. Conrad, and M. H. Shaevitz, Phys. Rev. Lett. **117**, 221801 (2016), [1607.00011](#).
- [67] S. Gariazzo, C. Giunti, M. Laveder, and Y. F. Li, JHEP **06**, 135 (2017), [1703.00860](#).
- [68] R. Gandhi, P. Ghoshal, S. Goswami, P. Mehta, and S. U. Sankar, Phys. Rev. **D73**, 053001 (2006), [hep-ph/0411252](#).
- [69] G. L. Fogli, E. Lisi, A. Marrone, D. Montanino, A. Palazzo, and A. M. Rotunno, Phys. Rev. **D86**, 013012 (2012), [1205.5254](#).
- [70] M. C. Gonzalez-Garcia, M. Maltoni, and T. Schwetz (2015), [1512.06856](#).
- [71] D. V. Forero, M. Tortola, and J. W. F. Valle, Phys. Rev. **D90**, 093006 (2014), [1405.7540](#).
- [72] K. Abe et al. (T2K) (2017), [1707.01048](#).
- [73] P. Adamson et al. (NOvA), Phys. Rev. Lett. **116**, 151806 (2016), [1601.05022](#).